Received: 16 July 2015 | Revised: 22 December 2017 | Accepted: 12 March 2018

DOI: 10.1002/oca.2431

RESEARCH ARTICLE

WILEY

A direct design method of controllers based on the frequency response indices for servo systems

Songlin Chen[1] | Ting Chen[2,3] | Kemao Ma[1] | Zongru He[1] | Yu Yao[1]

[1]Harbin Institute of Technology, Harbin 150080, China

[2]Innovation Academy for Microsatellites of CAS, Shanghai 201203, China,

[3]Shanghai Engineering Center for Microsatellites, Shanghai 201203, China

Correspondence
Songlin Chen, Control and Simulation Center, Harbin Institute of Technology, Harbin 150080, China.
Email: songlin@hit.edu.cn

Funding information
National Natural Science Foundation of China, Grant/Award Number: 61174001 and 61321062

Summary

To improve the design efficiency of servo systems, a novel controller design method is proposed based on the desired closed-loop transfer functions satisfying the required frequency response indices. Taking into account the constraint due to the physical realizability of controllers, the desired closed-loop transfer functions are specified. In addition, the analytical expressions for certain kinds of performance indices and design constraints, including dual-ten indices of frequency responses, crossover frequency, phase margin, and magnitude margin, are derived. Then, the principles for controller parameter determination are discussed. The controller design is formulated as an optimal problem with a variety of constraints, and the design guidelines are presented. At last, experiments are conducted to verify the effectiveness of the proposed method.

KEYWORDS

controller, direct design, frequency response indices, optimization, servo systems

1 | INTRODUCTION

With the rapid development of automation technology, servo systems are playing more and more important roles in various fields, such as industry, aerospace, navigation, and so on. Therefore, there has been an increasing interest in controller design methods of servo systems.[1-4]

The objective of control design is to provide a controller so that the closed-loop system satisfies desired performance indices. Among frequency response indices, the dual-ten frequency response indices, which reflect a system's tracking ability accurately, are adopted widely in high dynamic servo systems.[5,6] Due to the lack of quantitative design methods implementing dual-ten frequency response indices, control engineers have to conduct a trail-and-error design based on certain fundamental regulations and success or failure of the design depends heavily on personal experiences. In the traditional frequency-domain control design for high-performance servo systems, engineers would choose the crossover frequency via their experiences according to the desired dual-ten frequency response indices in the first step. Next, they design compensators to provide certain phase margin and magnitude margin at the crossover frequency, and then check if the performance of closed-loop system meets the requirements. Generally, it is not easy to reach a success for the closed-loop system, satisfying the performance specifications in the first trial. The main reason is that the quantitative relationships between the closed-loop behaviors and the open-loop characteristics determined by the controlled plant and the controller are not established during the control design. Consequently, the engineers have to adjust the structures and parameters of controllers repeatedly until the performance is satisfied over the whole considered frequencies. Such a trial-and-error design procedure leads to inefficiency, and the engineers' experiences greatly influence the efficiency of the design and the final performance. Therefore, to improve the efficiency of control design and to fully exploit

the performance potentials of a servo system, it is necessary to investigate controller design method into which the dual-ten frequency response indices are incorporated directly.

In the literature of direct method for control design, most of the attention is focused on sampled-data systems. Jiang and Lei[7] proposed a direct design method for digital controllers based on pole placement, the minimum beat control, and Dahlin algorithm, but the systems designed in this way are sensitive to parameter variations and the additional poles used to reduce overshoot of step response need be determined through simulation. Moreover, the relationships between the performance indices and the z-transform of the desired closed-loop response are not straightforward, causing difficulty in calculation.[8] The direct design methods for continuous controllers presented in other works[9-15] specified different desired closed-loop transfer functions for several common types of process models, and PI or PID controllers are derived by using either a series expansion or a frequency domain approximation. The methods can provide good performance in terms of disturbance rejection if the design parameters are selected properly, but the trial and error is indispensable because no quantitative relations between frequency response and the controller were established to facilitate parameter selection. Other analytical methods in other works[16-22] fixed the structure of the controller to be PID. Additionally, thereinto, Alcántara et al[16-18] addressed the servo/regulator and robustness/performance trade-off by analyzing the effect of an only parameter; Jin et al[19] designed a PID controller considering the maximum sensitivity and the integral square error criterion for step signals; Zhang et al[20] provided the quantitative time-domain responses while Zhang et al[21] presented the quantitative frequency responses including resonance peaks and stability margins for process control systems in a graphic way. Wang et al[22] designed a PID controller for the first-order velocity servo system to ensure that the frequency characteristic of the open-loop transfer function passes through 0 dB at a given frequency, and the desired phase margin is achieved. Goberdhansingh et al[23] proposed a control system design methodology based on a user-specified closed-loop transfer function. In this method, an iterative procedure is employed to minimize the sum of squared differences between the estimated and desired open-loop frequency responses for optimization of controller parameters. However, the quantitative design of closed-loop transfer function was not involved. Chee and Kang[24] studied the desired loop shape and design of an on-track mode controller. The desired loop shape is expressed as the performance shaping function, and the controller is designed using loop-shaping technique to maintain stability margins. However, this work paid more emphasis on stability instead of performance of the closed-loop system. Although those direct controller design methods reported in literature contributed a lot to control practice, few practical control design methods in terms of the dual-ten frequency response indices, to the best of our knowledge, have been reported so far.

This paper proposes a novel controller design procedure for servo systems based on dual-ten frequency response indices. The prominent advantage of the procedure is that the performance requirements are incorporated directly into control design to greatly improve both the efficiency of the design and the performance of the closed-loop systems. To begin, Section 2 expounds the basic idea of the direct method and analyzes the controller's physical realizability. Section 3 constructs the desired closed-loop transfer function for a servo system. The analytical expressions for certain performance indices and design constraints are derived in Section 4. The ways to evaluate the optimizing parameters are discussed and the optimization problem is formulated to solve the controller in Section 5. Experimental verification and the conclusion are presented, respectively, in Section 6 and Section 7.

2 | BASIC IDEA OF DIRECT METHOD AND THE CONTROLLER'S PHYSICAL REALIZABILITY

直接法的基本思想和物理可实现性

Consider a feedback control system with the standard block diagram in Figure 1, where $G(s)$ is the controlled plant and $K(s)$ is a controller, and, therefore the closed-loop transfer function is

$$\Phi(s) = \frac{K(s)G(s)}{1 + K(s)G(s)}. \quad \text{闭环传函} \tag{1}$$

If the desired closed-loop transfer function $\Phi_E(s)$ can be determined according to the given performance indices, then the corresponding controller can be calculated as follows:

$$K(s) = \frac{\Phi_E(s)}{G(s)\left(1 - \Phi_E(s)\right)}. \quad \text{控制器} \tag{2}$$

In this way, the controller design problem is equivalently transformed to the problem of constructing a desired closed-loop transfer function $\Phi_E(s)$. Given the requested performance, it is more direct to design the desired closed-loop transfer function $\Phi_E(s)$ rather than the controller $K(s)$, since the main performance indices are specified for the closed-loop system.

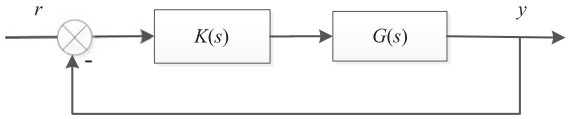

FIGURE 1 Block diagram of unity feedback control system

Before presenting a detailed method for designing $\Phi_E(s)$, we will analyze the relative degree constraint on the desired closed-loop transfer function, which guarantees that the controller to be derived is physically realizable. Rewrite the desired closed-loop transfer function and the controlled plant in terms of numerator and denominator polynomials as follows:

$$\Phi_E(s) = \frac{N_\Phi(s)}{M_\Phi(s)},\ G(s) = \frac{N_G(s)}{M_G(s)}.$$

Then

$$K(s) = \frac{N_\Phi(s)M_G(s)}{N_G(s)\left(M_\Phi(s) - N_\Phi(s)\right)}.$$

The corresponding degrees of the polynomials are specified as $\deg(N_\Phi)$, $\deg(M_\Phi)$, $\deg(N_G)$, and $\deg(M_G)$, respectively. Then, the physical realizability of the derived controller can be guaranteed if and only if the following inequality holds:

$$\deg(M_\Phi) + \deg(N_G) \geq \deg(N_\Phi) + \deg(M_G).$$

In other words, the constraint $\Delta D_\Phi \geq \Delta D_G$, where $\Delta D_\Phi = \deg(M_\Phi) - \deg(N_\Phi), \Delta D_G = \deg(M_G) - \deg(N_G)$, must be satisfied to ensure the controller's physical realizability when designing the desired closed-loop transfer function.

期望闭环传函设计

3 | DESIGN OF THE DESIRED CLOSED-LOOP TRANSFER FUNCTION

The controller for a servo system is usually expected to provide good tracking performance, ie, the amplitude of the desired closed-loop transfer function should be about one and the phase should be about zero in the interested frequency range. A second-order model with accurate parameters

$$\Phi_E(s) = \frac{{w_n}^2}{s^2 + 2\xi w_n s + {w_n}^2} \quad \text{二阶系统传函} \tag{3}$$

corresponds to the desired characteristic theoretically, and thus could be selected as the desired closed-loop transfer function.[25] Moreover, the two parameters, ie, w_n and ξ, could be determined according to performance indices.

Generally, a servo system driven by an electrical motor can be represented as[26]

$$G(s) = \frac{k_G}{s(\tau_e s + 1)(\tau_m s + 1)}, \quad \text{被控对象传函} \tag{4}$$

电气时间常数 机械时间常数

where k_G is the system gain and τ_e and τ_m are electrical time constant and the mechanical time constant, respectively. When the electrical time constant τ_e is very small and $1/\tau_e$ is much larger than the band width of the system, the controlled plant could be simplified as

$$G(s) = \frac{k_G}{s(\tau_m s + 1)}, \quad \text{简化被控对象} \tag{5}$$

with $\tau_m = J/B$, where J is the equivalent rotational inertia acting on the motor shaft and B is the equivalent damping. The controlled plant (5) could even be reduced to

$$G(s) = \frac{k_G}{Js^2} \quad \text{继续简化} \tag{6}$$

if the equivalent damping is negligible.

In case of the controlled plant is modeled as (5) or (6), the constraint $\Delta D_\Phi \geq \Delta D_G$ on the controllers realizability is equivalent to $\Delta D_\Phi \geq 2$, (3) meets the requirement and can be selected as the desired closed-loop transfer function.

To derive more general results, (4) will be taken as the nominal plant in this paper. In this case, substituting (3) and (4) to (2) gives the controller

$$K(s) = \frac{{w_n}^2(\tau_e s + 1)\,(\tau_m s + 1)}{k_G\,(s + 2\xi w_n)},$$

which is physically unrealizable, so the desired closed-loop transfer function must be modified. One feasible way is to introduce a first-order model with a time constant small enough compared with that of the original model (3). In this way, the desired closed-loop transfer function (3) is modified as follows:

$$\Phi_E(s) = \frac{{w_n}^2}{\left(s^2 + 2\xi w_n s + {w_n}^2\right)(Ts+1)} \tag{7}$$

and the corresponding realizable controller is expressed as

$$K(s) = \frac{{w_n}^2(\tau_e s+1)(\tau_m s+1)}{k_G\left(Ts^2 + (2T\xi w_n + 1)s + w_n(Tw_n + 2\xi)\right)}. \tag{8}$$

期望闭环传递函数的性能分析

4 | PERFORMANCE ANALYSIS OF THE DESIRED CLOSED-LOOP TRANSFER FUNCTION

For the desired closed-loop transfer function constructed in the previous section, the frequency responses are fully determined by its parameters. As a fact to be revealed in this section, various kinds of performance indices and design constraints, like dual-ten frequency response indices, crossover frequency, phase margin, and magnitude margin, are analytically related to those parameters in (7).

4.1 | Dual-ten indices

幅值误差小于10%，相位误差小于10 °

The dual-ten indices are among the most typical frequency-domain indices for high-performance servo systems, especially in the aerospace industry, which require that the amplitude error of a closed-loop transfer function be less than 10% and the phase error be less than 10°, both in given frequency band. In the following, the mathematical relationships between tracking error and parameters of the desired closed-loop transfer function will be analyzed.

4.1.1 | Amplitude error

The magnitude-frequency characteristic of the desired closed-loop transfer function (7) is

$$A(w) = \frac{{w_n}^2}{\sqrt{\left({w_n}^2 - w^2\right)^2 + (2\xi w_n w)^2}\sqrt{(Tw)^2+1}}. \tag{9}$$

It is necessary to figure out the monotonicity domains of $A(w)$ with respect to w and parameters, so that the highest frequency at which the amplitude error is less than 10% could be evaluated. Let $x = w^2$, and define

$$F(x) = f(x)\,g(x)$$

with

$$\begin{cases} f(x) = \left({w_n}^2 - x\right)^2 + (2\xi w_n)^2 x \\ g(x) = T^2 x + 1. \end{cases}$$

For quadratic function $f(x)$, the domain of definition is set to $x \in [0, +\infty)$, the discriminant is $\Delta_f = 16\xi^2 {w_n}^4(\xi^2 - 1)$, and the axis of symmetry is $x_f = {w_n}^2(1 - 2\xi^2)$. In addition, $f(0) = {w_n}^4 > 0$.

If $\xi \geq 1/\sqrt{2}$, $f(x)$ will increase monotonically in the domain of definition since $x_f = {w_n}^2(1 - 2\xi^2) \leq 0$, while $g(x)$ increases monotonically in the whole domain of definition, which means that the function $F(x)$ increases monotonically. Therefore, we can conclude that the magnitude-frequency characteristic (9) is monotonically decreasing when $\xi \geq 1/\sqrt{2}$.

However, the monotonicity becomes much more complicated if $0 \leq \xi < 1/\sqrt{2}$, and the corresponding results are shown in the Appendix.

Let the frequency corresponding the required dual-ten indices be specified as w_{fr}, the frequencies at which the magnitude reaches 1.1 and 0.9 for the first time be denoted by $w_{A1.1}$ and $w_{A0.9}$ accordingly, and the lowest frequency at which the amplitude error exceeds 10% be specified as w_A. It is easy to see that w_A is decided by $w_{A1.1}$ or $w_{A0.9}$ from the monotonicity of (9) and Figure 2. The analysis on various cases is conducted in the following.

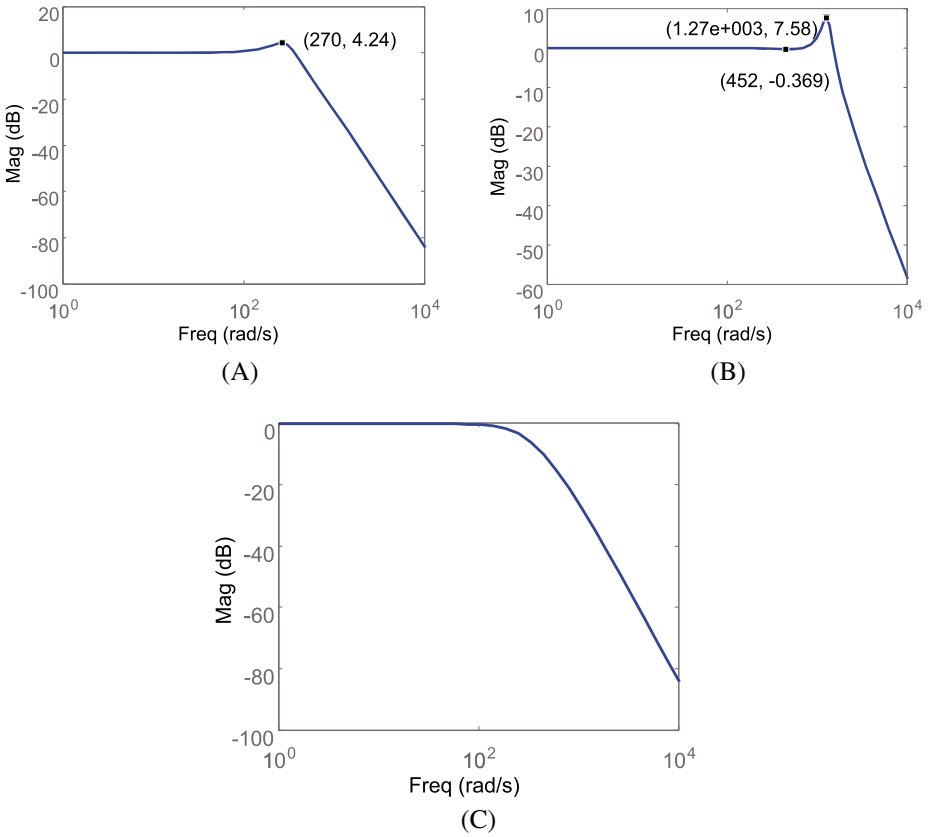

FIGURE 2 Monotonicity of closed-loop transfer function's magnitude. A, Increasing-Decreasing; B, Decreasing-Increasing-Decreasing; C, Monotonically decreasing [Colour figure can be viewed at wileyonlinelibrary.com]

In the case that the magnitude-frequency characteristic of the closed-loop transfer function is increasing-decreasing or decreasing-increasing-decreasing, as shown in Figures 2A and 2B, respectively, there is a resonant peak at the point

$$x_r = \frac{-b_r + \sqrt{\Delta_r}}{2a_r},$$

where

$$\begin{cases} a_r = 3T^2 \\ b_r = 2 - 4T^2 {w_n}^2 (1 - 2\xi^2) \\ \Delta_r = (4T^2 {w_n}^2 (1 - 2\xi^2) + 1)^2 - 3(4T^4 {w_n}^4 - 1) \end{cases}$$

and its response value is

$$M_r = \frac{{w_n}^2}{\sqrt{f(x_r)\left(\frac{\sqrt{\Delta_r}}{6} + \Omega\right)}} \tag{10}$$

with $\Omega = [2T^2 {w_n}^2 (1 - 2\xi^2) + 2]/3$.

On the other hand, if the magnitude-frequency characteristic of the closed-loop transfer function is decreasing-increasing-decreasing, there also is a minimum response value

$$A_{\min} = \frac{{w_n}^2}{\sqrt{f\left(x_{\min}\right)\left(-\frac{\sqrt{\Delta_r}}{6} + \Omega\right)}}$$

at the point

$$x_{\min} = \frac{-b_r - \sqrt{\Delta_r}}{2a_r}.$$

Therefore, there are two different situations involved to acquire w_A. Define

$$\begin{cases} a_s = T^2 \\ b_s = 1 - 2\left(1 - 2\xi^2\right) T^2 {w_n}^2 \\ c_s = w_n^2 \left[T^2 {w_n}^2 - 2\left(1 - 2\xi^2\right)\right] \\ d_s = \begin{cases} 21{w_n}^4/121, \text{when } A\left(w_A\right) = 1.1 \\ -19{w_n}^4/81, \text{when } A\left(w_A\right) = 0.9 \end{cases} \end{cases}$$

$$\begin{cases} A_s = {b_s}^2 - 3a_s c_s \\ B_s = b_s c_s - 9a_s d_s \\ C_s = {c_s}^2 - 3b_s d_s \\ \Psi_s = \frac{2A_s b_s - 3a_s B_s}{2\left(\sqrt{A_s}\right)^3} \\ \theta_s = \arccos \Psi_s \end{cases}$$

and $\Delta_{A0.9} = B_s^2 - 4A_s C_s$, and we have the following theorems to determine $w_{A1.1}$ and $w_{A0.9}$.

Theorem 1. *The highest frequency at which the magnitude of (7) is less than* 10% *is equal to* $w_{A1.1}$*, provided* $A_{\min} > 0.9$ *and* $M_r \geq 1.1$*, and the analytical expression for* $w_{A1.1}$ *is*

$$w_{A1.1} = \sqrt{\frac{-b_s + \sqrt{A_s}\left(\cos\left(\frac{\theta_s}{3}\right) - \sqrt{3}\sin\left(\frac{\theta_s}{3}\right)\right)}{3a_s}}.$$

Theorem 2. *The highest frequency at which the magnitude of (7) is less than* 10% *is equal to* $w_{A0.9}$ *if* $A_{\min} \leq 0.9$*, or* $A_{\min} > 0.9$ *and* $M_r < 1.1$*, or the magnitude is monotonically decreasing, and the analytical expression of* $w_{A0.9}$ *is as follows.*

1. *If* $\{\Delta_{A0.9} \geq 0, A_s \geq 0$ *or* $\begin{cases} \Delta_{A0.9} < 0 \\ A_{\min} > 0.9 \end{cases}$

$$w_{A0.9} = \sqrt{\frac{-b_s + \sqrt{A_s}\left(\cos\left(\frac{\theta_s}{3}\right) + \sqrt{3}\sin\left(\frac{\theta_s}{3}\right)\right)}{3a_s}}.$$

2. *If* $\Delta_{A0.9} \geq 0, A_s < 0$

$$w_{A0.9} = \sqrt{\frac{-b_s + \sqrt{A_s}\left(\cos\left(\frac{\theta_s}{3}\right) - \sqrt{3}\sin\left(\frac{\theta_s}{3}\right)\right)}{3a_s}}.$$

3. *If* $\Delta_{A0.9} < 0, A_{\min} \leq 0.9$

$$w_{A0.9} = \sqrt{\frac{-b_s - 2\sqrt{A_s}\cos\left(\frac{\theta_s}{3}\right)}{3a_s}}.$$

The detailed proof is omitted here.

With $T = 0.0014$ seconds, Figures 3 and 4 show the monotonicity of $w_{A0.9}$ and $w_{A1.1}$ with respect to w_n and ξ, respectively. As is seen, $w_{A0.9}$ increases with respect to w_n and decreases with respect to ξ, while $w_{A1.1}$ increases with respect to both w_n and ξ. Note that there is a $\bar{\xi}$ for every fixed w_n such that $w_{A1.1}$ does not exist when $\xi > \bar{\xi}$, which explains the discontinuity of the surface in Figure 4.

4.1.2 | Phase error

The phase-frequency characteristic of the desired closed-loop transfer function (7) is

$$\varphi(w) = -\tan^{-1}\frac{2\xi w_n w}{{w_n}^2 - w^2} - \tan^{-1}(Tw).$$

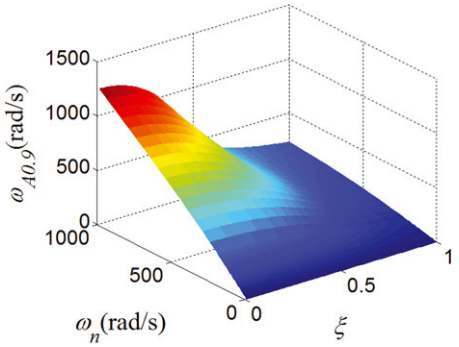

FIGURE 3 Monotonicity of $w_{A0.9}$ with respect to w_n and ξ [Colour figure can be viewed at wileyonlinelibrary.com]

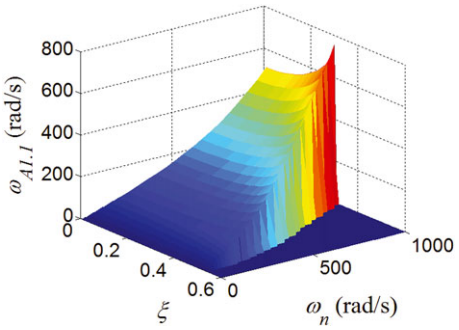

FIGURE 4 Monotonicity of $w_{A1.1}$ with respect to w_n and ξ [Colour figure can be viewed at wileyonlinelibrary.com]

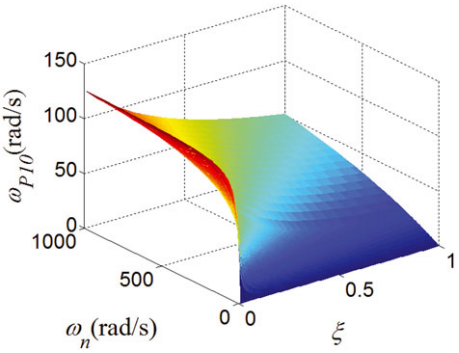

FIGURE 5 Monotonicity of $w_{P1.0}$ with respect to w_n and ξ [Colour figure can be viewed at wileyonlinelibrary.com]

Let the frequency at which the phase error reaches $-10°$ for the first time be w_{P10}. Due to the fact that $w_{P10} \ll w_n$ in most cases, omitting the term w^2 gives the simplified equation

$$\varphi(w_{P10}) = -\tan^{-1}\frac{2\xi w_{P10}}{w_n} - \tan^{-1}(Tw_{P10}).$$

It is easy to conclude that the phase decreases monotonically and is negative for all frequencies. Solving equation $\varphi(w_{P10}) = -10°$ results in

$$w_{P10} = \frac{\sqrt{(Tw_n + 2\xi)^2 + 8T\xi w_n \tan^2\left(\frac{\pi}{18}\right)} - (Tw_n + 2\xi)}{4T\xi \tan\left(\frac{\pi}{18}\right)}.$$

Monotonicity of w_{P10} with respect to w_n and ξ is shown in Figure 5 with $T = 0.0014$ seconds. To sum up, the system satisfies the required dual-ten indices if either of the following inequalities, per applicability, holds:

$$\begin{aligned} \min\{w_{A1.1}, w_{P10}\} &\geq w_{fr} \\ \min\{w_{A0.9}, w_{P10}\} &\geq w_{fr}. \end{aligned} \tag{11}$$

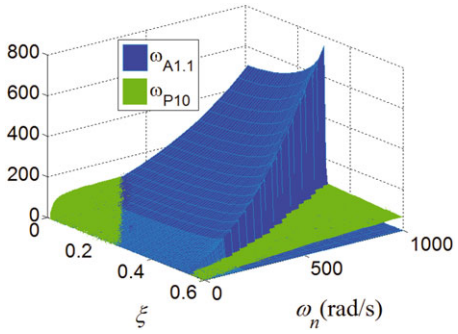

FIGURE 6 Comparison of $w_{A1.1}$ and w_{P10} [Colour figure can be viewed at wileyonlinelibrary.com]

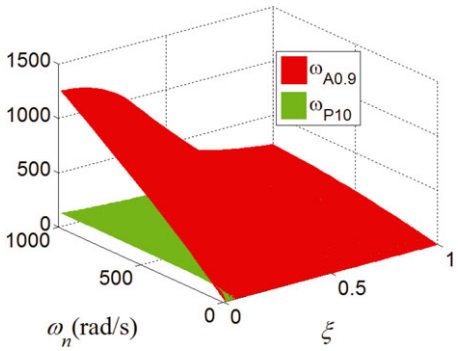

FIGURE 7 Comparison of $w_{A0.9}$ and w_{P10} [Colour figure can be viewed at wileyonlinelibrary.com]

Comparisons of $w_{A1.1}$ and w_{P10}, $w_{A0.9}$ and w_{P10} shown, respectively, in Figure 6 and Figure 7 present the relationship between the dual-ten frequency of a closed-loop system and its parameters (w_n and ξ) in an intuitive way.

It is noted that the highest frequency, which meets the requirement of dual-ten indices is given by w_{P10} with a rare exception in which both ξ and w_n are very small. Therefore, it is necessary to further analyze the monotonicity of w_{P10} with respect to ξ and w_n to the benefit of the accurate selection of parameters.

Theorem 3. *The frequency w_{P10} at which the phase error reaches $-10°$ for the first time is monotonically increasing with respect to $\frac{w_n}{\xi}$.*

Proof. Let $y = \frac{w_n}{\xi}$, then w_{P10} can be rewritten as $w_{P10} = \frac{h(y)}{4T\tan\frac{\pi}{18}}$, where

$$h\,(y) = \sqrt{(Ty+2)^2 + 8Ty\tan^2\left(\frac{\pi}{18}\right)} - (Ty+2).$$

Differentiate $h\,(y)$ with respect to y, and we get

$$h'(y) = \frac{T(Ty+2) + 8T\tan^2\left(\frac{\pi}{18}\right)}{\sqrt{(Ty+2)^2 + 8Ty\tan^2\left(\frac{\pi}{18}\right)}} - T,$$

which rewrites

$$h'(y) = \frac{\sqrt{T^2\left((Ty+2)^2 + 8Ty\tan^2\left(\frac{\pi}{18}\right)\right) + \Gamma}}{\sqrt{(Ty+2)^2 + 8Ty\tan^2\left(\frac{\pi}{18}\right)}} - T,$$

where $\Gamma = 64T^2\tan^2(\frac{\pi}{18})(1+\tan^2(\frac{\pi}{18}))$.

$h'(y) > 0$ for every $y > 0$, and thus $h(y)$ increases monotonically with respect to y. It is a good choice to increase $\frac{w_n}{\xi}$ to improve the dual-ten performance of the closed-loop system. □

Remark 1. Results on the dual-ten indices derived can be easily extended to dual-five, dual-three, or even other more complicated indices with different magnitude error and phase error requirements. The extension is straightforward but with some simple adjustments.

Remark 2. The parameter T could be set to zero to acquire more compact results when the relative degree of the controlled plant is less than three.

So far, the feasible region of w_n, ξ, and T could be determined according to (11) and the dual-ten indices. Other design constraints, like crossover frequency and stability margin, would help shrink the feasible region of those parameters and optimize them further.

4.2 | Crossover frequency

Limited by noise and high-frequency uncertainties in a real system, the crossover frequency could not be set too high actually, and instead, it should be as low as possible as long as the tracking performance is ensured. Thus, it is necessary to put some restriction on the crossover frequency.

Consider the open-loop transfer function derived from the desired closed-loop transfer function (7)

$$H(s) = \frac{{w_n}^2}{s\left(Ts^2 + (2T\xi w_n + 1)s + w_n(Tw_n + 2\xi)\right)}.$$

Specify the crossover frequency as w_c; then, the following equality

$$\frac{{w_n}^2}{w_c\sqrt{(2\xi w_n + T{w_n}^2 - T{w_c}^2)^2 + (2T\xi w_n + 1)^2 {w_c}^2}} = 1 \tag{12}$$

holds. Let $z = {w_c}^2$, and rewrite (12) to get $a_c z^3 + b_c z^2 + c_c z + d_c = 0$, where $a_c = T^2, b_c = 4\xi^2 T^2 {w_n}^2 - 2T^2 {w_n}^2 + 1, c_c = {w_n}^2(2\xi + Tw_n)^2$ and $d_c = -{w_n}^4$. Define

$$\begin{cases} A_c = b_c^2 - 3a_c c_c \\ B_c = b_c c_c - 9a_c d_c \\ C_c = c_c^2 - 3b_c d_c \\ M_c = \frac{2A_c b_c - 3a_c B_c}{2(\sqrt{A_c})^3} \\ \theta_c = \arccos M_c \end{cases}$$

and $\Delta_c = B_c^2 - 4A_c C_c$, then the analytical expression for w_c is as follows.

1. If $\Delta_c \geq 0, A_c \geq 0$

$$w_c = \sqrt{\frac{-b_c - 2\sqrt{A_c}\cos\left(\frac{\theta_c}{3}\right)}{3a_c}}.$$

2. If $\Delta_c \geq 0, A_c < 0$

$$w_c = \sqrt{\frac{-b_c + \sqrt{A_c}\left(\cos\left(\frac{\theta_c}{3}\right) - \sqrt{3}\sin\left(\frac{\theta_c}{3}\right)\right)}{3a_c}}.$$

3. If $\Delta_c < 0$

$$w_c = \sqrt{\frac{-b_c + \sqrt{A_c}\left(\cos\left(\frac{\theta_c}{3}\right) + \sqrt{3}\sin\left(\frac{\theta_c}{3}\right)\right)}{3a_c}}.$$

The monotonicity of crossover frequency w_c with respect to w_n and ξ is shown in Figure 8. w_c increases with respect to w_n, while it decreases with respect to ξ.

4.3 | Stability margin

For a control system, stability is a prerequisite to any other performance. Two significant stability criteria are the phase margin and the magnitude margin, which can guarantee the ability and resist perturbations in phase and magnitude, respectively.[27] Analysis on stability margin will be conducted to facilitate the parameters determination.

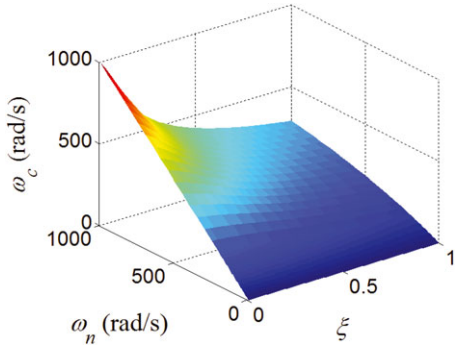

FIGURE 8 Monotonicity of crossover frequency with respect to w_n and ξ [Colour figure can be viewed at wileyonlinelibrary.com]

4.3.1 | Phase margin

Specifying the phase margin of the system as γ and substituting w_c derived in the previous section into the definition of phase margin,[28] we get the analytical expression of γ as follows:

$$\gamma = 90° - \tan^{-1}\frac{w_c\,(2T\xi w_n + 1)}{w_n\,(Tw_n + 2\xi) - Tw_c{}^2}.$$

The monotonicity of γ with respect to ξ differs greatly when w_n takes certain values in different ranges. Here, we consider only the range $0 < w_n < 1000$rad/s, which covers most of practical systems.

The monotonicity of phase margin γ with respect to w_n and ξ is shown in Figure 9. Higher phase margin could be achieved by increasing ξ.

4.3.2 | Magnitude margin

Define the frequency where the phase of open-loop system is $-180°$ as w_g, and let the magnitude margin be specified as k_g. Then, k_g could be derived by connecting the definition of magnitude margin with Routh law.[28]

First, it is assumed that the system turns marginally stable when the open-loop gain increases to K_1. The corresponding open-loop transfer function is

$$H_1(s) = \frac{K_1}{s\,(Ts^2 + (2T\xi w_n + 1)s + w_n(Tw_n + 2\xi))}$$

and its characteristic equation is

$$\frac{T}{w_n\,(Tw_n + 2\xi)}s^3 + \frac{2T\xi w_n + 1}{w_n\,(Tw_n + 2\xi)}s^2 + s + K_1 = 0.$$

Then, apply Routh law to obtain the necessary and sufficient condition of marginal stability as follows:

$$K_1 = \frac{2T\xi w_n + 1}{T}.$$

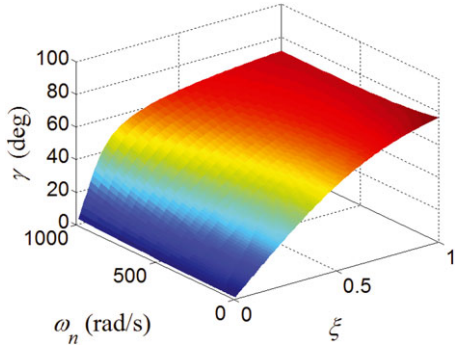

FIGURE 9 Monotonicity of phase margin γ with respect to w_n and ξ [Colour figure can be viewed at wileyonlinelibrary.com]

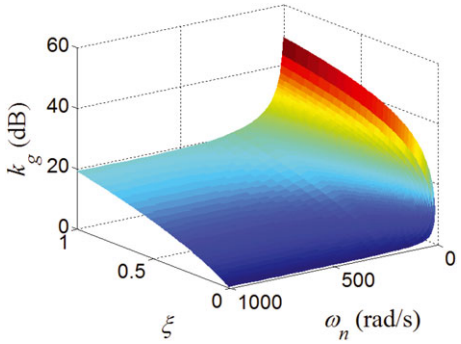

FIGURE 10 Monotonicity of magnitude margin k_g with respect to w_n and ξ [Colour figure can be viewed at wileyonlinelibrary.com]

By the definition of magnitude margin, the following equality holds:

$$K_1 = \frac{w_n}{Tw_n + 2\xi} k_g.$$

Therefore, the analytical expression of magnitude margin is

$$k_g = \frac{(2T\xi w_n + 1)(Tw_n + 2\xi)}{Tw_n}, \tag{13}$$

which rewrites as follows:

$$k_g = 4\xi^2 + 2T\xi w_n + \frac{2\xi}{Tw_n} + 1. \tag{14}$$

The monotonicity of magnitude margin k_g with respect to w_n and ξ is shown in Figure 10. Analysis in the previous section shows that $\frac{w_n}{\xi}$ should be increased to improve the dual-ten indices. In addition, inspired by (14), to increase w_n and ξ simultaneously with same rate is a feasible way to achieve a higher phase margin without deteriorating the dual-ten performance.

5 | OPTIMIZATION OF PERFORMANCE SPECIFICATIONS AND GUIDELINES FOR CONTROLLER DESIGN

With the help of the derived analytical expressions of dual-ten frequency, crossover frequency, phase margin, and amplitude margin, the feasible region of parameters could be located according to prescribed performance specifications and design constraints. In this way, further optimization algorithm needs to be developed to optimize parameters.

It is clarified that $\frac{w_n}{\xi}$ should be increased to improve the dual-ten performance while ξ is increased with a fixed w_n to achieve a higher phase margin. Trade-off must be made inevitably between these two performance indices, so two trade-off optimizations are proposed in this section.

5.1 | Optimization for phase margin with certain dual-ten indices and magnitude margin

First, the phase margin can be taken as optimal objective to determine the parameters of the desired closed-loop transfer function while the dual-ten indices, crossover frequency, and magnitude margin are specified as design constraints. In this case, the controller design can be formulated as an optimal problem with a variety of constraints as follows:

$$\min_{\boldsymbol{\lambda}_m \le \boldsymbol{\lambda} \le \boldsymbol{\lambda}_M} \{-\gamma(\boldsymbol{\lambda})\}$$
$$\text{s.t.} \begin{bmatrix} w_{fr} - w_s(\boldsymbol{\lambda}) \\ k_{gr} - k_g(\boldsymbol{\lambda}) \\ w_c(\boldsymbol{\lambda}) - w_{c\max} \end{bmatrix} \le 0, \tag{15}$$

where $\gamma(\boldsymbol{\lambda}) = 90° - \tan^{-1} \frac{w_c(2T\xi w_n + 1)}{w_n(Tw_n + 2\xi) - Tw_c^2}$ with ω_c given by Section 4.2; $\boldsymbol{\lambda} = [\ w_n \ \ \xi\ ]$ is the optimizing vector with the lower boundary $\boldsymbol{\lambda}_m = [0\ 0]$ and upper boundary $\boldsymbol{\lambda}_M = [\ 1000 \ \ 1\ ]$; $w_s(\boldsymbol{\lambda})$ and $k_g(\boldsymbol{\lambda})$ represent the dual-ten frequency and magnitude margin, respectively; $w_c(\boldsymbol{\lambda})$ denotes the crossover frequency with the upper bound $w_{c\max}$ imposed by high-frequency uncertainty; w_{fr} and k_{gr} are the required dual-ten indices frequency and the required magnitude margin, respectively.

The optimal parameter vector $\boldsymbol{\lambda}^*$ could be obtained by applying the function *fmincon*, an optimization solver in MATLAB, which can find minimum of a constrained nonlinear multivariable function. For more detail, please refer to the works of MathWorks.[29,30]

5.2 | Optimization for the dual-ten indices with certain phase margin and magnitude margin

On the other hand, the dual-ten performance can be optimized while taking crossover frequency, phase margin, and magnitude margin as design constraints, which can improve the tracking ability of the system. In this way, the controller design is formulated as the following optimization problem:

$$\begin{aligned} &\min_{\boldsymbol{\lambda}_m \le \boldsymbol{\lambda} \le \boldsymbol{\lambda}_M} \{-w_s(\boldsymbol{\lambda})\} \\ &\text{s.t.} \begin{bmatrix} \gamma_r - \gamma(\boldsymbol{\lambda}) \\ k_{gr} - k_g(\boldsymbol{\lambda}) \\ w_c(\boldsymbol{\lambda}) - w_{c\max} \end{bmatrix} \le 0, \end{aligned} \tag{16}$$

where γ_r represents the required phase margin and

$$\omega_s(\boldsymbol{\lambda}) = \begin{cases} \omega_{A1.1} & \text{if } A_{\min} > 0.9 \text{ and } M_r \ge 1.1 \\ \omega_{A0.9} & \text{if } A_{\min} \le 0.9 \text{ or } A_{\min} > 0.9 \text{ and } M_r < 1.1 \end{cases}$$

with $\omega_{A1.1}$ given by Theorem 1 and $\omega_{A0.9}$ given by Theorem 2.

The optimal parameter vector $\boldsymbol{\lambda}^*$, which could also be derived via function fmincon, corresponds to the optimal dual-ten frequency under given constraints.

5.3 | Guidelines for controller design

The guidelines of controller design are summed up as follows.

1. Construct the transfer function of the controlled plant. Model the transfer function of controlled plant in either form of (4), (5), or (6) according to specific circumstances, and determine the model parameters via system identification or simply taking their values.
2. Design the desired transfer function. First, set T as a relatively small constant $T_0 > 0$, or $T = 0$ if the controlled plant is of second order, and then determine optimal parameters w_n^* and ξ^* by solving the optimization problem (15) or (16) in accordance with specific design preference.
3. Derive the controller. Substitute the transfer function of controlled plant and the desired closed-loop transfer function into (2) to yield the controller $K(s)$, which will readily satisfy the performance indices.

6 | EXPERIMENTAL VERIFICATION

To validate the effectiveness and practicality of the proposed direct design method of controllers, we apply it to the interior axis of triaxial flight simulator shown in Figure 11. The triaxial flight simulator consists of frames, motors and their inverters, encoders, and controller. The frames are made of aluminum alloy whose low density helps reduce the moment of inertia; permanent magnet synchronous motors are used as actuators and Germany-made KEB F5S inverters are employed to drive the motors; Germany-made Heidenhain photoelectric encoders are used as angle transducer. The model of the encoder used in the interior axis is RON786C and its resolution is 0.0001°. The controller is implemented via a 610H industrial computer made by Taiwan Advantech. In this computer, a PCL-726 D/A conversion card is installed to send torque command to inverters, and a PCL-1784 counter card is installed to receive angle feedback from encoders. We developed a program to implement the control algorithms by using Visual C++ 6.0. This program runs on RTX8.1, which is a realtime extended subsystem for Windows XP. The control period is 0.5 ms.

The required performance specifications are as follows.

1. Dual-ten frequency is no less than 9 Hz.
2. Magnitude margin is no less than 5 dB.
3. Crossover frequency is no higher than 50 Hz.

FIGURE 11 The triaxial flight simulator used in the research [Colour figure can be viewed at wileyonlinelibrary.com]

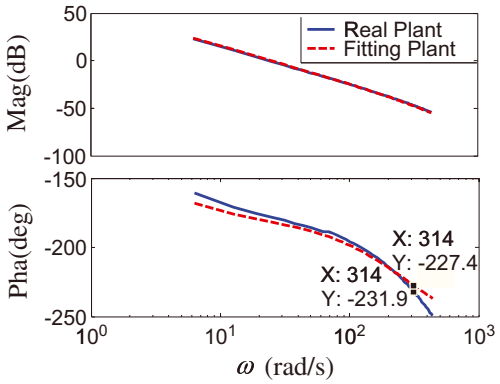

FIGURE 12 Bode diagram of the controlled plant [Colour figure can be viewed at wileyonlinelibrary.com]

According to the guidelines for controller design shown in Section 5, we choose (4) as the accurate description of the plant's dynamics so as to obtain higher performance. By inputting sine signals with different frequencies, we obtained the frequency characteristic of the interior axis shown in Figure 12 in solid line. Based on the model (4) and the obtained frequency characteristic, the least squares method is used to identify the system parameters, and the complete model is described as

$$G(s) = \frac{434}{s\,(0.0035s + 1)\,(0.67s + 1)},$$

whose frequency characteristic curve is shown in Figure 12 in dashed line. We can see that the frequency characteristics of the fitting model and the real plant match well in the frequency range of interest.

Furthermore, we set $T = 0.0014$ seconds, $\lambda_0 = [316, 0.6]$ with lower bound $\lambda_l = [0, 0]$ and upper bound $\lambda_u = [1000, 1]$, and the corresponding corner frequency is about 100 Hz, which has little impact on the performance within 9 Hz. We take dual-ten indices, magnitude margin, and crossover frequency as control constraints and apply the first case in Section 5.1, ie, the optimization of the phase margin. The optimal parameters are obtained as $\xi^* = 0.2807$, $w_n^* = 405.4322$ rad/s, and the desired closed-loop transfer function is

$$\Phi_E(s) = \frac{164375.2706}{(s^2 + 227.61s + 164375.2706)(0.0014s + 1)}.$$

Finally, substitute $G(s)$ and $\Phi_E(s)$ into (2) and we have the controller

$$K(s) = \frac{164375.2706(0.0035s + 1)(0.67s + 1)}{434(0.0014s^2 + 1.3187s + 457.7607)}. \tag{17}$$

Bode diagrams of the open-loop system and closed-loop system are shown in Figure 13 and Figure 14, respectively. It can be seen that the crossover frequency is $w_c = 50$ Hz, magnitude margin is k_g= 8.5dB, phase margin is $\gamma = 37°$, and the dual-ten frequency is $w_s = 60$rad/s ≈ 9.5Hz, which shows that all the performance requirements are met. Meanwhile, the dual-ten frequency is equal to w_{P10}, consistent with the analysis in previous sections.

To verify the effectiveness and practicality of the proposed direct design method, the controller (17) is discretized using Tustin approach with the sampling period 0.5 ms. Then, the tracking curves to sine signals with amplitude 0.5 degree and frequencies 1 Hz, 3 Hz, 6 Hz, and 9 Hz are shown in Figure 15, and the numerical comparison of theoretical and

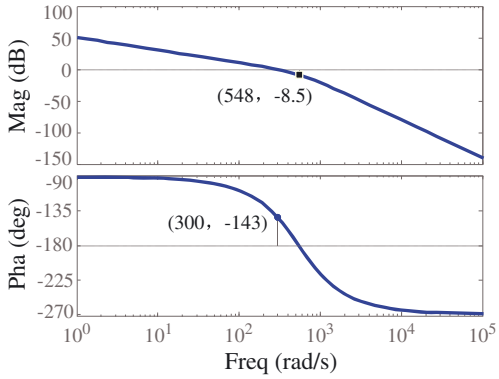

FIGURE 13 Bode diagram of the open-loop system [Colour figure can be viewed at wileyonlinelibrary.com]

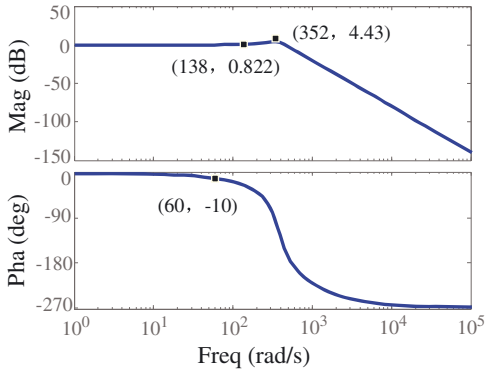

FIGURE 14 Bode diagram of the closed-loop system [Colour figure can be viewed at wileyonlinelibrary.com]

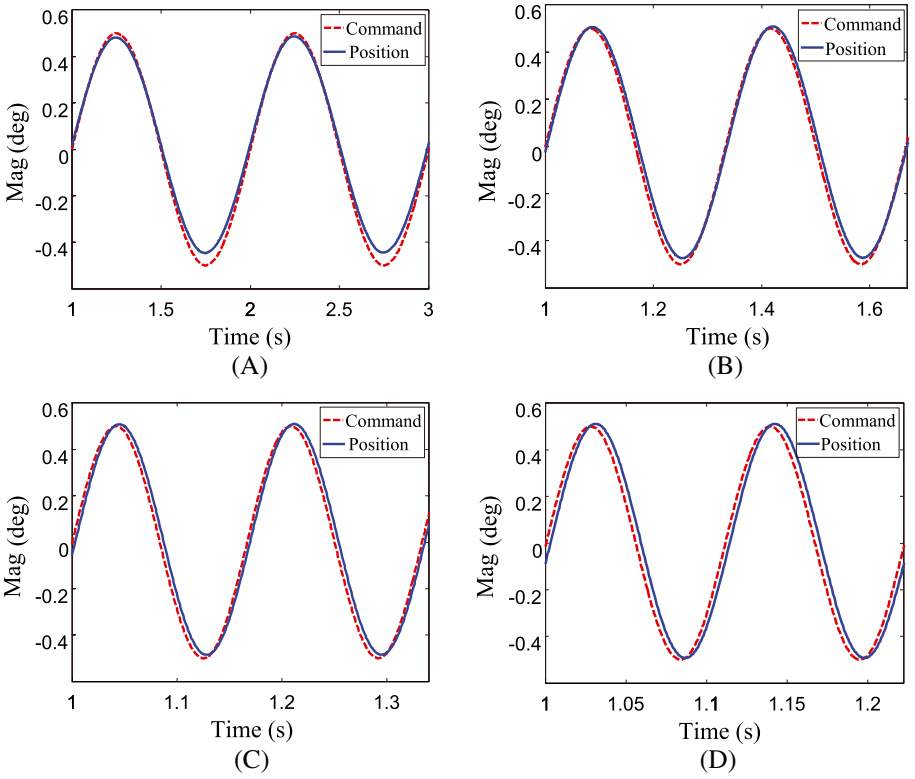

FIGURE 15 Sinusoidal response of the actual system with controller (17) (a) $w = 1$Hz; (b) $w = 3$Hz; (c) $w = 6$Hz; (d) $w = 9$Hz [Colour figure can be viewed at wileyonlinelibrary.com]

TABLE 1 Comparison between theoretical and experimental results of sinusoidal responses with controller (17)

w (Hz)	FFT mag		FFT phase (deg)	
	Theoretical values	Experimental values	Theoretical values	Experimental values
1	1.0002	0.9315	-1.1705	0.252
2	1.0007	0.9681	-1.9982	-2.374
3	1.0015	0.9813	-3.0233	-4.153
4	1.0027	0.9866	-4.0347	-5.110
5	1.0042	0.9908	-5.0239	-5.974
6	1.0062	0.9944	-6.1183	-6.856
7	1.0083	0.9976	-7.1081	-7.746
8	1.0109	1.0009	-8.1480	-8.715
9	1.0137	1.0039	-9.1372	-9.705

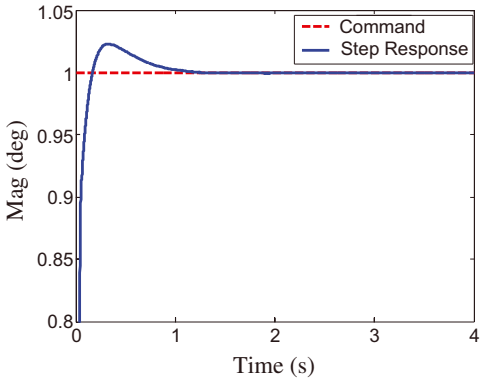

FIGURE 16 Step response of the closed-loop system [Colour figure can be viewed at wileyonlinelibrary.com]

experimental results of sinusoidal responses (derived via FFT of input and output data) are shown in Table 1. It is shown that the experimental results conform to the theoretical results, and the slight deviation, especially at low frequencies, is understandable in view of the friction in the system, difference between the nominal plant and the real plant, and error caused by controller discretization, and so on.

The response to a step input with amplitude one degree is conducted to test performance of the closed-loop system from another point of view, and the experiment result is shown in Figure 16. The overshoot is 2.3% and the adjusting time is very short, which indicates superior tracking performance and dynamic stability. Actually, the step response in experiment is different from the one in numerical simulation, which has an overshoot of 33% and oscillations due to the low value of ξ. Some nonlinear features in the real system, such as friction, dead zone, saturation, and so on, can explain such differences. For example, the friction will increase the systems damp equivalently, which consequently decreases the overshoot and oscillations of the step response.

Furthermore, we continue to verify the effectiveness of the second case presented in Section 5.2. We take phase margin (no less than 32°), magnitude margin, and crossover frequency as control constraints and apply the second optimization algorithm to improve the dual-ten indices. Using the same initial conditions, the optimal parameters are obtained as $\xi^* = 0.2328$ and $\omega_n^* = 380.4278\text{rad/s}$. Consequently, the desired closed-loop transfer function is

$$\Phi_E(s) = \frac{144730}{(s^2 + 177.1272s + 144730)(0.0014s + 1)}.$$

In addition, the corresponding controller is

$$K(s) = \frac{144730(0.0035s + 1)(0.67s + 1)}{434(0.0014s^2 + 1.2480s + 379.7426)}. \tag{18}$$

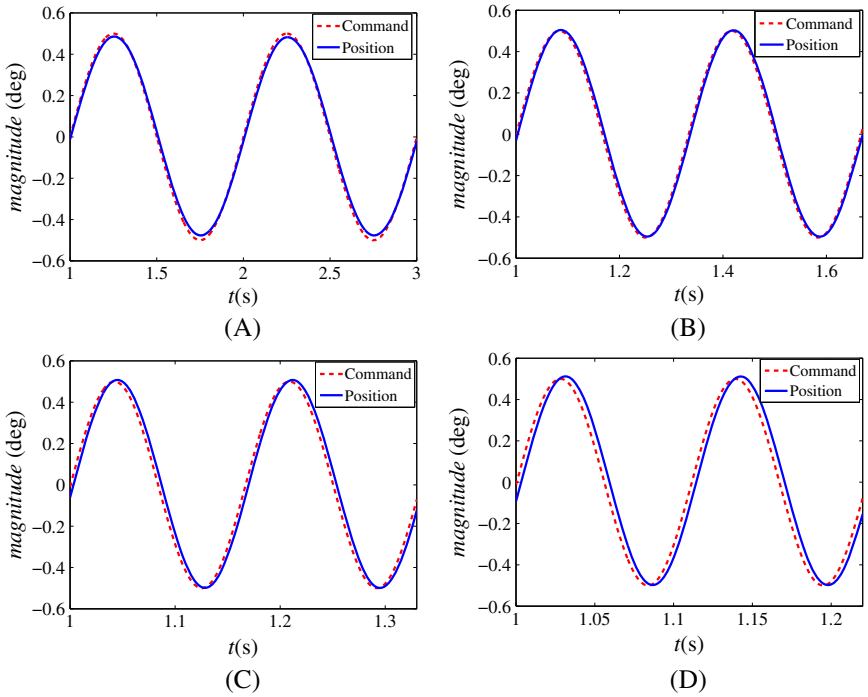

FIGURE 17 Sinusoidal response of the actual system with controller (18). A, $w = 1$ Hz; B, $w = 3$ Hz; C, $w = 6$ Hz; D, $w = 9$ Hz [Colour figure can be viewed at wileyonlinelibrary.com]

TABLE 2 Comparison between theoretical and experimental results of sinusoidal responses with controller (18)

w (Hz)	FFT mag		FFT phase (deg)	
	Theoretical values	Experimental values	Theoretical values	Experimental values
1	1.0002	0.9626	-0.9447	-2.58
2	1.0008	0.9937	-1.8900	-2.92
3	1.0018	1.0000	-2.8365	-3.72
4	1.0033	1.0030	-3.7847	-4.68
5	1.0051	0.0052	-4.7354	-5.54
6	1.0074	1.0069	-5.6891	-6.40
7	1.0101	1.0087	-6.6464	-7.32
8	1.0133	1.0103	-7.6081	-8.21
9	1.0169	1.0113	-8.5748	-9.13
10	1.0209	1.0149	-9.5472	-9.96

By calculation, we can get that the crossover frequency is $\omega_c = 50$ Hz, the magnitude margin is $k_g = 7.43$ dB, the phase margin is $\gamma = 32.1°$, and the dual-ten frequency is $\omega_s = 65.7$ rad/s ≈ 10.46 Hz, which means all the performance requirements are met. Similar to the optimization of phase margin, the dual-ten frequency is equal to w_{P10}, too. It can be observed that the dual-ten indices are enhanced with about 1 Hz at cost of a loss of about 5° in the phase margin.

To verify the effectiveness and practicality of the controller (18), we carry out same experiments of the controller (17). The tracking curves to sine signals with amplitude 0.5 degree and frequencies 1 Hz, 3 Hz, 6 Hz, and 9Hz are shown in Figure 17, and the numerical comparison of theoretical and experimental results of sinusoidal responses are shown in Table 2. As we can see, the experimental results conform to the theoretical results. However, similar to the case of the controller (17), the unmodeled dynamics in actual system result in the slight deviation between theoretical and experimental results.

7 | CONCLUSION

A novel method of controller design based on dual-ten frequency response indices has been developed for servo systems. By specifying the desired closed-loop transfer function properly, the analytical expressions for several kinds of performance indices are derived, and the controller design is formulated as nonlinear optimization problems with a variety of constraints. The proposed controller design method takes into account directly the dual-ten frequency response indices to improve the design efficiency and employs the optimization algorithms to improve the system performance. The effectiveness of the proposed method is sufficiently demonstrated by the experiments conducted on a flight simulation turntable.

It can be expected that the performance of a system can be further improved if the desired closed-loop transfer function with different generally more complicated forms is employed to provide more degrees of freedom for optimization. We will consider this expectation in our further work. Considering that this proposed method is strongly dependent on accurate models and there exist inevitably various uncertainties in real systems, we will also investigate the improvement of the robustness of the controller design method.

ACKNOWLEDGEMENT

This work was partially supported by the National Natural Science Foundation of China under grants 61174001 and 61321062.

ORCID

Songlin Chen http://orcid.org/0000-0002-3030-4393

REFERENCES

1. Chen BM, Lee TH, Peng K, Venkataramanan V. *Hard Disk Drive Servo Systems*. London, UK: Springer-Verlag London; 2006.
2. Iwasaki M, Seki K, Maeda Y. High-precision motion control techniques: a promising approach to improving motion performance. *IEEE Ind Electron Mag*. 2012;6(1):32-40.
3. Lyshevski SE. Nonlinear control of servo-systems actuated by permanent-magnet synchronous motors. *Automatica*. 1998;34(10):1231-1238.
4. Zhong G, Shao Z, Deng H, Ren J. Precise position synchronous control for multi-axis servo systems. *IEEE Trans Ind Electron*. 2017;64(5):3707-3717.
5. Fang HY. *Simulation of Air Defense Missile Weapon System [M]*. Beijing, China: China Astronautic Publishing House; 1995. (in Chinese).
6. Xiao PZ, Lin QS. Research of the dynamic performance of DC servo control system based on fractional order $PI^{\lambda}D^{\mu}$. Paper presented at: 2013 IEEE International Conference on Advanced Mechatronic Syst (ICAMechS); 2013; Luoyang, China.
7. Jiang J, Lei Y. Direct design of digital controller on frequency domain specification. *J HeBei Inst Mechano-Electric Eng*. 1996;13(2):1-6. (in Chinese).
8. Dou D. Some properties of digital system with direct design controller on z domain. *J ZheJiang Inst Tech*. 1984;2:78-89. (in Chinese).
9. Chen D, Seborg DE. PI/PID controller design based on direct synthesis and disturbance rejection. *Ind Eng Chem Res*. 2002;41(19):4807-4822.
10. Rao AS, Rao V, Chidambaram M. Direct synthesis-based controller design for integrating processes with time delay. *J Franklin Inst*. 2009;346(1):38-56.
11. Hu W, Xiao G, Cai W-J. PID controller design based on two-degrees-of-freedom direct synthesis. Paper presented at: 2011 Chinese Control and Decision Conference (CCDC); 2011; Mianyang, China.
12. Xiang X, Li W, Liu Q, Xu J, Ma Y. Model and control for inner loop of electro-optical tracking servo system. Paper presented at: 2014 IEEE International Conference on Mechatronics and Automation (ICMA); 2014; Tianjin, China.
13. Gopi P, Rao K, Subramanyam M, Satyaprasad K. Design of internal model control-proportional integral derivative controller with improved filter for disturbance rejection. *Syst Sci Control Eng: An Open Access J*. 2014;2(1):583-592.
14. Vanavil B, Chaitanya KK, Rao AS. Improved PID controller design for unstable time delay processes based on direct synthesis method and maximum sensitivity. *Int J Syst Sci*. 2013;46(8):1-18.
15. Panda RC. Synthesis of PID tuning rule using the desired closed-loop response. *Ind Eng Chem Res*. 2008;47(22):8684-8692.
16. Alcántara S, Pedret C, Vilanova R. On the model matching approach to PID design: analytical perspective for robust servo/regulator tradeoff tuning. *J Process Control*. 2010;20(5):596-608.
17. Alcántara S, Zhang WD, Pedret C, Vilanova R, Skogestad S. IMC-like analytical H^{∞} design with S/SP mixed sensitivity consideration: utility in PID tuning guidance. *J Process Control*. 2011;21(6):976-985.
18. Alcántara S, Vilanova R, Pedret C. PID control in terms of robustness/performance and servo/regulator trade-offs: a unifying approach to balanced autotuning. *J Process Control*. 2013;23(4):527-542.

19. Jin Q-B, Liu Q, Wang Q, Li S-N, Wang Z. IMC–PID design: analytical optimization for performance/robustness tradeoff tuning for servo/regulation mode. *Asian J Control*. 2014;16(4):1252-1261.
20. Zhang W, Xi Y, Yang G, Xu X. Design PID controllers for desired time-domain or frequency-domain response. *ISA Trans*. 2002;41(4):511-520.
21. Zhang W, Xu X, Sun Y. Quantitative performance design for integrating processes with time delay. *Automatica*. 1999;35(4):719-723.
22. Wang C, Fu W, Shi Y. An analytical design of fractional order proportional integral differential controller for robust velocity servo. Paper presented at: 25th Chinese Control and Decision Conference (CCDC); 2013; Guiyang, China.
23. Goberdhansingh E, Wang L, Cluett W. Robust control system design using direct frequency response. Paper presented at: 1992 American Control Conference; 1992; Chicago, IL.
24. Chee W, Kang C. Practical frequency shaping of on-track mode controller of HDD servo. *IEEE Trans Magn*. 1999;35(5):2277-2279.
25. Lin R, Zhou Y, Chen L. Fast and automatic design of regulators in continuous control system. *J Autom*. 1985;11:132-137. (in Chinese).
26. Mei X, Bo G, Zhang M. *Automatic Control Components and Circuit*. Beijing, China: Science Press; 2007. (in Chinese).
27. Nie Z. *The Gain and Phase Margins Calculation and Controllers Design* [dissertation]. Changsha, China: Central South University; 2012. (in Chinese).
28. Hu S. *Principles of Automatic Control*. Beijing: National Defense Industry Press; 1994. (in Chinese).
29. https://www.mathworks.com/help/optim/ug/fmincon.html?s_tid=srchtitle
30. Optimisation Toolbox™ User's Guide for MATLAB 2016b. Natick, MA: The MathWorks, Inc; 2016.

How to cite this article: Chen S, Chen T, Ma K, He Z, Yao Y. A direct design method of controllers based on the frequency response indices for servo systems. *Optim Control Appl Meth*. 2018;1–18. https://doi.org/10.1002/oca.2431

APPENDIX

TABLE A1 Magnitude monotonicity of the desired closed-loop transfer function in Equation (7)

Case	Monotonically Decreasing	Increasing-Decreasing	Decreasing-Increasing-Decreasing
A	$\begin{cases} T^2{w_n}^2 > 2\Phi \\ 0 < \xi < \frac{1}{2} \\ \Phi \le \frac{\sqrt{3(4T^4{w_n}^4-1)}-1}{4T^2{w_n}^2} \end{cases}$	$\begin{cases} T^2{w_n}^2 < \frac{1}{2\Phi} \\ 0 < \xi < \frac{1}{2} \end{cases}$	$\begin{cases} T^2{w_n}^2 > 2\Phi \\ 0 < \xi < \frac{1}{2} \\ \Phi > \frac{\sqrt{3(4T^4{w_n}^4-1)}-1}{4T^2{w_n}^2} \end{cases}$
B	$\begin{cases} T^2{w_n}^2 > \frac{1}{2\Phi} \\ \frac{1}{2} \le \xi < \frac{1}{\sqrt{2}} \\ \Phi \le \frac{\sqrt{3(4T^4{w_n}^4-1)}-1}{4T^2{w_n}^2} \end{cases}$	$\begin{cases} T^2{w_n}^2 < 2\Phi \\ \frac{1}{2} \le \xi < \frac{1}{\sqrt{2}} \end{cases}$	$\begin{cases} T^2{w_n}^2 > \frac{1}{2\Phi} \\ \frac{1}{2} \le \xi < \frac{1}{\sqrt{2}} \\ \Phi > \frac{\sqrt{3(4T^4{w_n}^4-1)}-1}{4T^2{w_n}^2} \end{cases}$
C	$2\Phi \le T^2{w_n}^2 < \frac{1}{2\Phi}$	$\frac{1}{2\Phi} \le T^2{w_n}^2 < 2\Phi$	–
D	$\xi \ge \frac{1}{\sqrt{2}}$	–	–

Note: $\Phi = 1 - 2\xi^2$.